PHOTONICS Research

Nonlinear silicon photonics on CMOS-compatible tellurium oxide

Neetesh Singh,[1,2,*] Hamidu M. Mbonde,[3] Henry C. Frankis,[3] Erich Ippen,[2] Jonathan D. B. Bradley,[3,4] and Franz X. Kärtner[1]

[1]Centre for Free Electron Laser Science (CFEL)-DESY and University of Hamburg, 22607 Hamburg, Germany
[2]Research Laboratory of Electronics, Massachusetts Institute of Technology, Cambridge, Massachusetts 02139, USA
[3]Department of Engineering Physics, McMaster University, Hamilton, Ontario L8S 4L7, Canada
[4]e-mail: jbradley@mcmaster.ca
*Corresponding author: neeteshs@mit.edu

Received 23 June 2020; revised 29 September 2020; accepted 18 October 2020; posted 19 October 2020 (Doc. ID 400057); published 30 November 2020

Silicon photonics is coming of age; however, it is still lacking a monolithic platform for optical sources and nonlinear functionalities prompting heterogeneous integration of different materials tailored to different applications. Here we demonstrate tellurium oxide as a complementary metal oxide semiconductor silicon photonics platform for nonlinear functionalities, which is already becoming an established platform for sources and amplifiers. We show broadband supercontinuum generation covering the entire telecom window and show for the first time to our knowledge third-harmonic generation in its integrated embodiment. Together with the now-available lasers and amplifiers on integrated TeO_2 this work paves the way for a monolithic TeO_2-based nonlinear silicon photonics platform.

https://doi.org/10.1364/PRJ.400057

1. INTRODUCTION

Silicon photonics is reaching its maturity in terms of passive and active optoelectronic functionalities. However, monolithic integration of light sources and nonlinear optical devices is still an ambitious goal. Silicon cannot be electrically pumped due to its indirect band gap, and it cannot be optically pumped due to its low solubility of rare-earth ions [1,2]. There has been significant progress with electrically pumped III-V material as sources on silicon photonics platforms and recently as nonlinear optics platforms [3,4]; however, they tend to be expensive, thermally instable, and have low yield [1,5,6]. On the other hand, for nonlinear photonics, silicon has a very high Kerr factor, 200–400 times that of silica, leading to various demonstrations [7–12]. However, it suffers from high two-photon absorption in the telecom band due to being too close to the band gap [13]. This compels researchers to operate either at longer wavelengths, which is far away from the band gap, or employ new material platforms having higher band-gap energy [8,14–16]. One such material that has received significant attention recently is silicon nitride, which has been used routinely for generating over an octave spanning supercontinuum [17–19]. The Kerr factor of the stoichiometric silicon nitride (Si_3N_4) is only 10 times that of silica [20,21] and thus requires high pump power, but such a limitation can be relaxed with silicon rich silicon nitride, albeit with the increase in propagation losses and reduction of the band-gap energy, which thus makes it susceptible to nonlinear absorption [21,22]. Most importantly, however, silicon nitride has not been demonstrated as a reliable host material for rare-earth gain to allow monolithic integration of sources and optical nonlinear functionalities.

A rare-earth-doped medium is an excellent candidate for monolithic integration of an optically pumped laser, and there have been many demonstrations recently of high-power integrated lasers [23–27]. However, the host material used in these works tends to have low optical nonlinearity, which thus limits its applicability as a nonlinear medium. Tellurium oxide (TeO_2) is an excellent candidate for monolithic integration of optical sources and linear and nonlinear functionalities in silicon photonics without incurring nonlinear absorption loss. As a source it is establishing itself as a host medium for various rare-earth ions, offering opportunities for amplifiers and lasers at many wavelengths [28–30]. Furthermore, it has highly desirable material properties, such as a high refractive index of 2.1 at 1550 nm and high nonlinearity—Kerr coefficients up to 30 to 50 times that of silica [30–33]. Its Raman coefficient is 60 times that of silica and demonstrates extremely strong second-order optical nonlinearity for a glass [34–37]. Due to these excellent optical properties it has been used to generate over 2.6 octaves of supercontinuum in sub-centimeter photonic crystal fiber [38]. However, fabrication of integrated tellurium oxide has been challenging thus far. In the first half of the last two

decades, there were significant attempts at fabricating TeO_2 waveguides, for example, using femtosecond laser writing, ion exchange, ion implantation, and reactive ion etching methods [33,39–42]. However, for nonlinear photonics, such devices have had limited success either due to high propagation loss, weak guidance, or large mode area of the pump limiting the overall optical intensity for efficient nonlinear signal conversion.

In this work, we demonstrate strong nonlinear effects in TeO_2 utilizing a different waveguide fabrication technique that avoids any etching or implantation and thus reduces the propagation loss significantly while maintaining small mode area, ensuring high optical intensity in the core [43]. We achieve coherent supercontinuum (SC) generation over the entire telecom band in the normal dispersion regime, which is a factor of 10 broader than the previous demonstration over a decade ago [33]. Such a device has applications, for example, in few-cycle pulse generation and optical coherence tomography [44,45]. We also demonstrate, to the best of our knowledge, for the first time third-harmonic generation (THG) in an integrated TeO_2 platform with tens of nanowatts of signal strength. This demonstration opens possibilities for on-chip pulse diagnostics [46] and efficient and coherent short pulse generation on chip in the wavelength windows where lasers are not readily available. We utilize room-temperature deposition of TeO_2 to fabricate waveguides and thus make them fully compatible with the back-end-of-the-line CMOS electronic processes. Furthermore, we show how a thicker layer of TeO_2 can be fabricated for obtaining anomalous dispersion for generating SC over an octave. Such a device not only is useful as a stand-alone highly nonlinear system but can also enhance the nonlinearity of the existing Si_3N_4 waveguides postfabrication. Together with the emerging integrated lasers and amplifiers on TeO_2 and other rare-earth media [47–49,24,25], this work paves the way for a monolithic TeO_2-based nonlinear silicon photonics platform.

2. RESULTS

We have designed and fabricated a silicon nitride waveguide of 200 nm thickness (t), 1200 nm width (w), and 7 mm length with low-pressure chemical vapor deposition (LPCVD) in a standard wafer scale foundry (Lionix). The waveguide was then deposited with tellurium oxide (TeO_2) in house using a radio frequency reactive sputtering technique to a thickness (l_d) of 370 nm as shown in Fig. 1. The deposition rate and the temperature were 20 nm/min and 20°C, respectively. At 1550 nm the refractive index of 2.08 was measured with a spectroscopic ellipsometer, and the film loss of 0.1 dB/cm was measured with the prism coupling technique (Metricon). The propagation loss of the waveguide was around 0.5 dB/cm, based on the measurements that can be found in Refs. [43,49]. A 3 μm thick top cladding (Cytop, $n = 1.33$ at 1550 nm) was spin coated as a protection layer. We note that the coupling loss was as high as ~15 dB/facet, mainly due to imperfect polishing of the facets (Ultrapol polisher); therefore, inverse tapers will be used in future devices to reduce coupling loss. Although we used LPCVD for depositing Si_3N_4, which requires processing temperature around 800°C and thus making it incompatible with the back-end-of-the-line (BEOL) CMOS processes [19,50,51], to make the device fully compatible with CMOS electronics we can equally use the well-established plasma-enhanced chemical vapor deposition (PECVD)-based silicon nitride layer [19,24,50,51]. The schematic of the waveguide cross section and an SEM image are shown in Figs. 1(b) and 1(c).

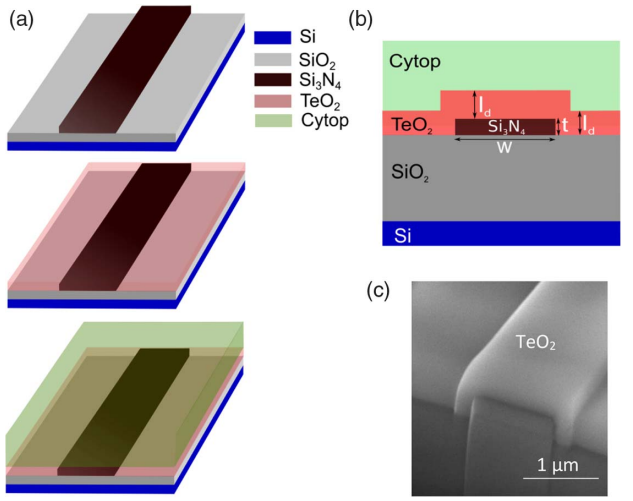

Fig. 1. (a) Schematic of the waveguide fabrication steps with different layers. (b) Schematic of the waveguide cross section. (c) SEM image of the waveguide.

We calculated the dispersion and the effective index of the waveguide, shown in Fig. 2(a), using a commercial finite-difference-based mode solver (Lumerical) for the fundamental TE mode, as it offers stronger confinement. The dispersion is normal at 1550 nm with $\beta_2 = 0.27$ ps^2/m, $\beta_3 = -9.2 \times 10^{-40}$ s^3/m, $\beta_4 = 5.58 \times 10^{-54}$ s^4/m, and $\beta_5 = -2.46 \times 10^{-68}$ s^5/m. We note that the dispersion variation due to the rounding of the corners of the TeO_2 layer of the fabricated device, seen in Fig. 1(c), was negligible. The fundamental mode profile at 1550 nm is shown in Fig. 2(b) with 70% of the total energy confined in the tellurium oxide. The nonlinearity (γ) of the waveguide was approximately twice higher than that of a waveguide made of only silicon nitride (oxide cladded) with similar dimensions, i.e., height of 570 nm and width of 1.2 μm. Here, the γ can be approximately defined as $2\pi[rn_{2t} + (1-r)n_{2s}]/\lambda a_{\text{eff}}$, where r is the percentage of energy present in tellurium oxide and n_{2t} and n_s are the Kerr coefficients of tellurium oxide and LPCVD silicon nitride, which are 10×10^{-19} m^2/W and 2.4×10^{-19} m^2/W, respectively. We note here that the Kerr factor of tellurium oxide varies within 30–50 times that of silica in literature [31–33,52]; therefore, with consideration of our results of SC generation, we have used the tellurium oxide's Kerr factor to be up to 42 times that of the silica in the simulations. Here λ and a_{eff} are the wavelength and the effective area (1.3 μm^2) of the pump. For comparison, in Fig. 2(c) the mode profile of a silica-clad silicon nitride waveguide is shown, having mode area of 2 μm^2, where a significant amount of the mode is overlapping with the cladding silica layer.

In the experiment, the waveguide was pumped with an optical parametric oscillator generating pulses of 200 fs width at

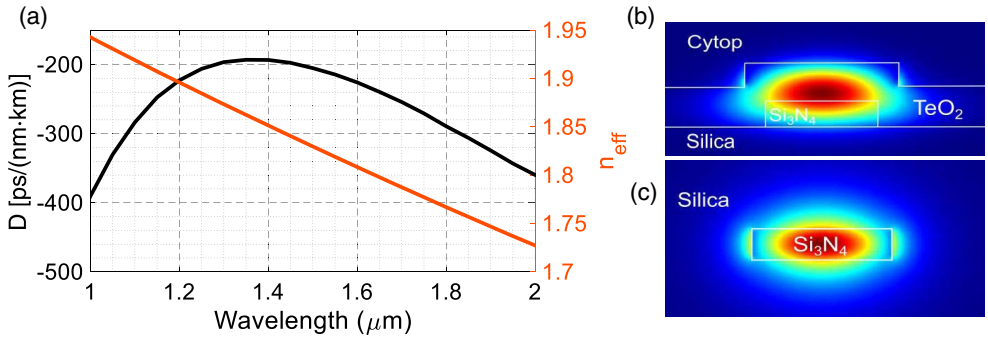

Fig. 2. (a) Calculated dispersion and effective index of the waveguide for the fundamental TE mode. (b) and (c) The mode profile at 1550 nm of the waveguide with and without tellurium oxide, respectively.

1550 nm, at a repetition rate of 80 MHz. The peak power coupled into the waveguide was estimated to be 600 W. The output was collected by butt coupling a multimode fluoride fiber connected to an optical spectrum analyzer. The self-phase-modulation-based SC generation spectrum is shown in Fig. 3, spanning around 1550 nm over 500 nm at −30 dB level from the peak, which is 10 times broader than in the previous demonstration [33], without showing any signs of damage at high power levels for hours of operation. The SC was simulated by solving the well-known nonlinear Schrodinger equation with the split-step Fourier method [53]. We experimentally observed the THG in the visible wavelength range. THG, which has been observed in many media and platforms [54–63], requires interaction of three pump photons in a nonlinear material to generate one signal photon. It requires phase matching between the pump and the signal and efficient overlap of the respective modes, normally involving the fundamental mode of the pump and higher-order or radiation modes of the signal [64,65].

We measured the third-harmonic signal at around 517 nm as shown in Fig. 3. The on-chip signal strength was approximately 100 nW for 10 mW of average power of the pump. In Fig. 4 the SC and the THG at different pump powers are shown. The difference between the third-harmonic signal strength for the pump peak power of 420 W and 300 W is 5 dB and for the pump power of 420 W and 150 W is 15 dB, which is in accordance with the THG relation $I_3 \sim I_1^3$ [64], where I_1 and I_3 are the intensities of the pump and the signal, respectively. The expected on-chip efficiency for the current unoptimized waveguide is $(P_{3w}/P_w) > 2 \times 10^{-3}\%$, where P_{3w} and P_w are the peak power of the signal and the pump respectively. A higher THG power can be obtained by suppressing SC broadening using longer pump pulses and optimizing the waveguide design for strong overlap and phase matching between the pump and the signal modes. The exact mode of the third-harmonic signal for the presented work is currently being investigated, which, regardless of the type, is mostly confined in the TeO_2 films (as seen in the

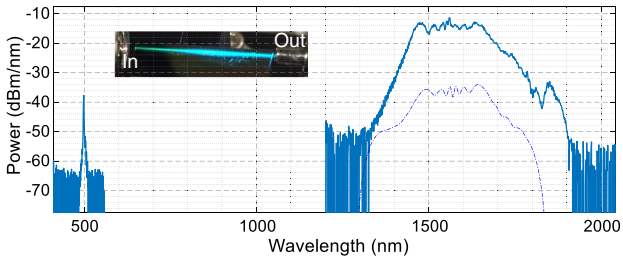

Fig. 3. Experimental supercontinuum and third-harmonic generation spectra with an image of the third-harmonic generation along the length of the waveguide (inset). The vertical axis is on-chip power, and the dashed curve is the simulated spectrum shifted down for clarity.

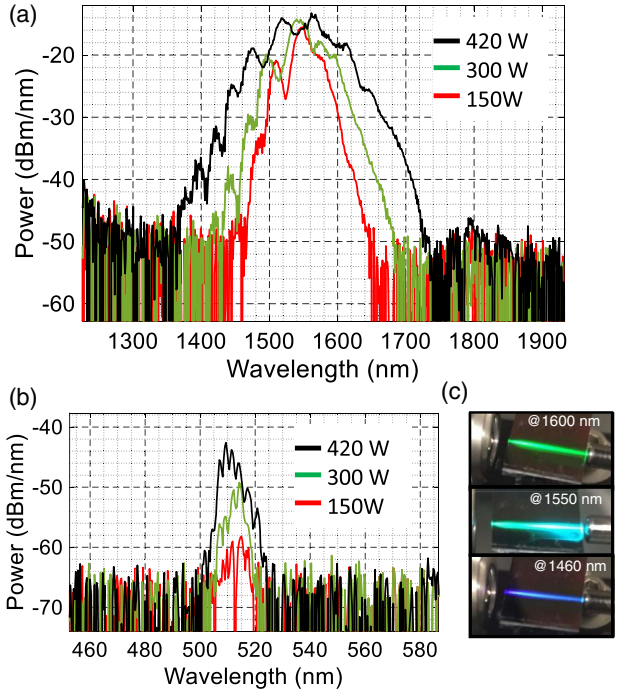

Fig. 4. (a) and (b) The supercontinuum and third-harmonic generation spectra at different pump powers. (c) Optical images, taken with a CMOS camera, of third-harmonic generation at different pump wavelengths with signal color of green (pump at 1600 nm), cyan (pump at 1550 nm), and blue (pump at 1460 nm). The input is at the left side of the images. The third-harmonic signal had larger scattering for the 1550 nm pump (inset), as the pump power was higher than for the others.

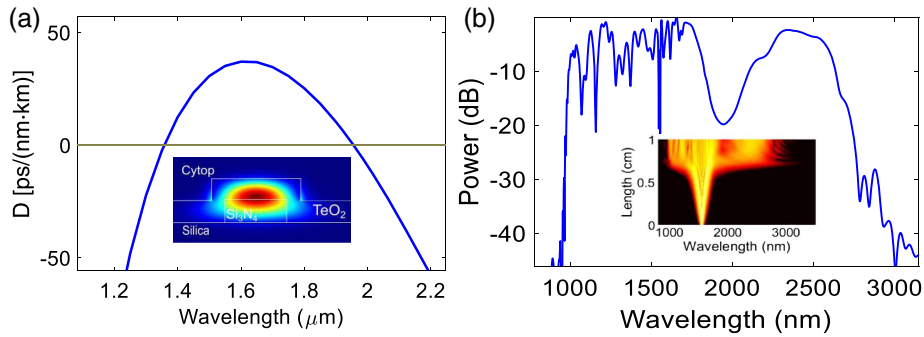

Fig. 5. (a) Calculated anomalous dispersion of the waveguide and the mode profile for the fundamental TE mode (inset). Energy confined in silicon nitride is ~30%. (b) Calculated supercontinuum generation along with the spectrogram (inset) for a 1 cm long waveguide at 1 kW of pump power at 1550 nm.

simulations); thus, the propagation loss in the visible is estimated to be between 1 and 2 dB/cm [43]. The THG along the length of the waveguide for different pump wavelengths captured with a CMOS camera is also shown in Fig. 4(c).

Furthermore, we show a design to generate a soliton-fission-based SC spanning over an octave, which is crucial for various applications including optical frequency synthesis based on carrier envelope phase stabilization [66]. In this design a thicker Si_3N_4 layer is used (~450 nm), with a width of 1.2 μm, over which a 450 nm of tellurium oxide is deposited. The TE mode of the pump and the dispersion of the waveguide are shown in Fig. 5(a). The first zero-dispersion wavelength (ZDW) is around 1.35 μm, and the second ZDW is at 1.95 μm. Although a thicker silicon nitride leads to a reduction in nonlinearity, as the energy confined in the Si_3N_4 is relatively large ~30%, it helps obtain anomalous dispersion with the type of waveguide cross section used in this work [67].

In the SC simulation we launched a 200 fs pulse with 1 kW of peak power at 1550 nm into a 1 cm long waveguide. The SC spectrum is shown in Fig. 5(b), where the signal spans from 1 to 2.7 μm at −20 dB level from the peak. The soliton fission happens around 7 mm propagation length and generates a strong dispersive wave beyond the second ZDW around 2.45 μm. The waveguide can be modified further to have strong dispersive wave signals in the visible and in the deep mid-IR range with a nonuniform waveguide design [68], as the transparency bandwidth of tellurium spans from 400 nm to 6 μm.

In conclusion, we have demonstrated strong SC generation in a highly nonlinear TeO_2 waveguide, in the normal dispersion regime around 1550 nm, which has applications, for example, in optical coherence tomography and few-cycle pulse generation, as the pulse splitting is avoided and the coherence of the pulse is maintained. We also demonstrated, for the first time to our knowledge, THG on an integrated platform of TeO_2, which was observed at the visible wavelengths that can be used as a coherent short pulse source in the visible spectrum on a CMOS platform. Although the TeO_2 waveguide is demonstrated here as a stand-alone device, it can very well be used for postfabrication enhancement of the nonlinearity of existing silicon nitride or silicon waveguides. This work makes TeO_2 a potential CMOS-compatible nonlinear silicon photonics material that, together with the integrated TeO_2-based lasers and amplifiers, paves the way for full monolithic integration in silicon photonics.

Funding. Defense Advanced Research Projects Agency (HR0011-15-C-0056); Natural Sciences and Engineering Research Council of Canada (RGPIN-2017-06423, STPGP 494306); Deutsche Forschungsgemeinschaft (SP2111).

Disclosures. The authors declare no conflicts of interest.

REFERENCES

1. Z. Zhou, B. Yin, and J. Michel, "On-chip light sources for silicon photonics," Light Sci. Appl. **4**, e358 (2015).
2. A. J. Kenyon, "Erbium in silicon," Semicond. Sci. Technol. **20**, R65–R84 (2005).
3. U. D. Dave, C. Ciret, S. P. Gorza, S. Combrie, A. D. Rossi, F. Raineri, G. Roelkens, and B. Kuyken, "Dispersive-wave-based octave-spanning supercontinuum generation in InGaP membrane waveguides on a silicon substrate," Opt. Lett. **40**, 3584–3587 (2015).
4. M. Pu, L. Ottaviano, E. Semenova, and K. Yvind, "Efficient frequency comb generation in AlGaAs-on-insulator," Optica **3**, 823–826 (2016).
5. D. Liang and J. E. Bowers, "Recent progress in lasers on silicon," Nat. Photonics **4**, 511–517 (2010).
6. B. Stern, X. Ji, Y. Okawachi, A. L. Gaeta, and M. Lipson, "Battery-operated integrated frequency comb generator," Nature **562**, 401–405 (2018).
7. A. D. Bristow, N. Rotenber, and H. M. van Driel, "Two photon absorption and Kerr coefficients of silicon for 850–2200 nm," Appl. Phys. Lett. **90**, 191104 (2007).
8. N. Singh, M. Xing, D. Vermeulen, K. Shtyrkova, N. Li, P. T. Callahan, E. S. Magden, A. Ruocco, N. Fahrenkopf, Ch. Baiocco, B. P.-P. Kuo, S. Radic, E. P. Ippen, F. X. Kärtner, and M. R. Watts, "Octave-spanning coherent supercontinuum generation in silicon on insulator from 1.06 μm to beyond 2.4 μm," Light Sci. Appl. **7**, 17131 (2018).
9. M. A. Foster, A. C. Turner, J. E. Sharping, B. S. Schmidt, M. Lipson, and A. L. Gaeta, "Broad-band optical parametric gain on a silicon photonic chip," Nature **441**, 960–963 (2006).
10. N. Singh, M. Raval, A. Ruocco, and M. R. Watts, "Broadband 200 nm second harmonic generation in silicon in the telecom band," Light Sci. Appl. **9**, 17 (2020).
11. J. Leuthold, "Nonlinear silicon photonics," Nat. photonics **4**, 535–544 (2010).
12. B. Kuyken, X. Liu, R. M. Osgood, R. Baets, G. Roelkens, and W. M. J. Green, "Mid-infrared to telecom-band supercontinuum generation in highly nonlinear silicon-on-insulator wire waveguides," Opt. Express **19**, 20172–20181 (2011).
13. M. Sheik-bahae and E. W. van Stryland, "Optical nonlinearities in the transparency region of bulk semiconductor," Semiconduct. Semimetals **58**, 257–318 (1998).

14. N. Singh, D. D. Hudson, Y. Yu, C. Grillet, S. D. Jackson, A. C. Bedoya, A. Read, P. Atanackovic, S. G. Duvall, S. Palomba, B. L. Davies, S. Madden, D. J. Moss, and B. J. Eggleton, "Mid infrared supercontinuum generation from 2 to 6 μm in a silicon nanowire," Optica **2**, 797–802 (2015).
15. N. Nader, A. Kowligy, J. Chiles, E. J. Stanton, H. Timmers, A. J. Lind, F. C. Cruz, D. M. B. Lesko, K. A. Briggman, S. W. Nam, S. A. Diddams, and R. P. Mirlin, "Infrared frequency comb generation and spectroscopy with suspended silicon nanophotonic waveguides," Optica **6**, 1269–1276 (2020).
16. B. Kuyken, T. Ideguchi, S. Holzner, M. Yan, T. W. Hänsch, J. V. Campenhout, P. Verheyen, S. Coen, F. Leo, R. Baets, G. Roelkens, and N. Picque, "An octave-spanning mid-infrared frequency comb generated in a silicon nanophotonic wire waveguide," Nat. Commun. **6**, 6310 (2015).
17. M. H. P. Pfeiffer, C. Herkommer, J. Liu, H. Guo, M. Karpov, E. Lucas, M. Zervas, and T. J. Kippenberg, "Octave-spanning dissipative Kerr soliton frequency combs in Si_3N_4 microresonators," Optica **4**, 684–691 (2017).
18. Y. Okawachi, M. Yu, J. Cardenas, X. Ji, A. Klenner, M. Lipson, and A. L. Gaeta, "Carrier envelope offset detection via simultaneous supercontinuum and second-harmonic generation in a silicon nitride waveguide," Opt. Lett. **43**, 4627–4630 (2018).
19. J. Chiles, N. Nadar, D. D. Hickstein, S. P. Yu, T. C. Briles, D. Carlson, H. Jung, J. M. Shainline, S. Diddams, S. B. Papp, S. W. Nam, and R. P. Mirlin, "Deuterated silicon nitride photonic devices for broadband optical frequency comb generation," Opt. Lett. **43**, 1527–1530 (2018).
20. K. Ikeda, R. E. Saperstein, N. Alic, and Y. Fainman, "Thermal and Kerr properties of plasma deposited silicon nitride/silicon dioxide waveguides," Opt. Express **16**, 12987–12994 (2008).
21. C. Lacava, S. Stankovic, A. Z. Khokar, T. D. Bucio, F. Y. Gardes, G. T. Reed, D. J. Richardson, and P. Petropoulos, "Si-rich silicon nitride for nonlinear signal processing applications," Sci. Rep. **7**, 22 (2016).
22. D. T. H. Tan, K. J. A. Ooi, and D. K. T. Ng, "Nonlinear optics on silicon-rich nitride—a high nonlinear figure of merit CMOS platform," Photon. Res. **6**, B50–B66 (2018).
23. E. S. Hosseini, J. D. B. Bradley, J. Sun, G. Leake, T. N. Adams, D. D. Coolbaugh, and M. R. Watts, "CMOS-compatible 75 mW erbium-doped distributed feedback laser," Opt. Lett. **39**, 3106–3109 (2014).
24. K. Shtyrkova, P. T. Callahan, N. Li, E. S. Magden, A. Ruocco, D. Vermeulen, F. X. Kartner, M. R. Watts, and E. P. Ippen, "Integrated CMOS-compatible *Q*-switched modelocked lasers at 1900 nm with an on-chip artificial saturable absorber," Opt. Express **27**, 3542–3556 (2019).
25. N. Singh, E. Ippen, and F. X. Kartner, "Towards CW modelocked laser on chip—a large mode area and NLI for stretched pulse mode locking," Opt. Express **28**, 22562–22579 (2020).
26. N. Li, D. Vermeulen, Z. Su, E. S. Magden, M. Xin, N. Singh, A. Ruocco, J. Notaros, C. V. Poulton, E. Timurdogan, C. Baiocco, and M. R. Watts, "Monolithically integrated erbium doped tunable laser on a CMOS-compatible silicon photonics platform," Opt. Express **26**, 16200–16211 (2018).
27. E. S. Magden, N. Li, J. D. B. Bradley, N. Singh, A. Ruocco, G. S. Petrich, G. Leake, D. D. Coolbaugh, E. P. Ippen, M. R. Watts, and L. A. Kolodzieski, "Monolithically-integrated distributed feedback laser compatible with CMOS processing," Opt. Express **25**, 18058–18065 (2017).
28. M. Yamada, A. Mori, K. Kobayashi, H. Ono, T. Kanamori, K. Oikawa, Y. Nishida, and Y. Ohishi, "Gain flattened tellurite based EDFA with a flat amplification bandwidth of 76 nm," IEEE Photon. Technol. Lett. **10**, 1244–1246 (1998).
29. A. Jha, S. Shaoxiong, L. H. Huang, and P. Joshi, "Spectroscopic properties of rare earth metal ion doped tellurium oxide glasses and fibres," J. Opt. **33**, 157–170 (2004).
30. S. Shen, A. Jha, X. Liu, and M. Naftaly, "Tellurite glasses for broadband amplifiers and integrated optics," J. Am. Ceram. Soc. **85**, 1391–1395 (2002).
31. S. H. Kim, T. Yoko, and S. Sakka, "Linear and nonlinear optical properties of TeO_2 glass," J. Am. Ceram. Soc. **76**, 2486–2490 (1993).
32. S. H. Kim and T. Yoko, "Nonlinear optical properties of TeO_2-based glasses: MO_x-TeO_2 (M = Sc, Ti, V, Nb, Mo, Ta, and W) binary glasses," J. Am. Ceram. Soc. **78**, 1061–1065 (1995).
33. S. J. Madden and K. T. Vu, "Very low loss reactively ion etched Tellurium Dioxide planar rib waveguides for linear and non-linear optics," Opt. Express **17**, 17645–17651 (2009).
34. J. Rajan and O. Yasutake, "Higher nonlinear indices, Raman gain coefficients, and bandwidths in the TeO_2-ZnO-Nb_2O_5-MoO_3 quaternary glass system," Appl. Phys. Lett. **90**, 211104 (2007).
35. R. Stegeman, C. Rivero, K. Richardson, G. Stegman, P. Delfyett, Y. Guo, A. Pope, A. Schulte, T. Cardinal, P. Thomas, and J. C. C. Mesjard, "Raman gain measurements of thallium-tellurium oxide glasses," Opt. Express **13**, 1144–1149 (2005).
36. L. Kassab, R. Pinto, R. Kobayashi, M. Piasecki, P. Bragiel, and I. Kityk, "Photoinduced second-order optical susceptibilities of Er_2O_3 doped TeO_2–GeO_2–PbO glasses," Opt. Commun. **274**, 461–465 (2007).
37. T. Cheng, Y. Xiao, S. Li, X. Yan, X. Zhang, T. Suzuki, and Y. Ohishi, "Highly efficient second-harmonic generation in a tellurite optical fiber," Opt. Lett. **44**, 4686–4689 (2019).
38. P. Domachuk, N. A. Wolchover, M. Cronin-Golomb, A. Wang, A. K. George, C. M. B. Cordiero, J. C. Knight, and F. G. Omenetto, "Over 4000 nm bandwidth of mid-IR supercontinuum generation in sub-centimeter segments of highly nonlinear tellurite PCFs," Opt. Express **16**, 7161–7168 (2008).
39. P. Nandi, G. Jose, C. Jayakrishnan, S. Debbarma, K. Chalapathi, K. Alti, A. K. Dharmadhikari, J. A. Dharmadhikari, and D. Mathur, "Femtosecond laser written channel waveguides in tellurite glass," Opt. Express **14**, 12145–12150 (2006).
40. G. N. Conti, V. K. Tikhomirov, M. Bettinelli, S. Berneschi, M. Brenci, B. Chen, S. Pelli, A. Speghini, A. B. Seddon, and G. C. Righini, "Characterization of ion-exchanged waveguides in tungsten tellurite and zinc tellurite Er^{3+} doped glasses," Opt. Eng. **42**, 2805–2811 (2003).
41. G. N. Conti, S. Berneschi, M. Bettinelli, M. Brenci, B. Chen, S. Pelli, A. Speghini, and G. Righini, "Rare-earth doped tungsten tellurite glasses and waveguides: fabrication and characterization," J. Non Cryst. Solids **345**, 343–348 (2004).
42. S. Berneschi, M. Brenci, G. Nunzi Conti, S. Pelli, G. C. Righini, I. Bányász, A. Watterich, N. Khanh, M. Fried, and F. Pászti, "Channel waveguide fabrication in Er^{3+} doped tellurite glass by ion beam irradiation," Proc. SPIE **6475**, 647509 (2007).
43. H. C. Frankis, K. M. Kiani, D. B. Bonneville, C. Zhang, S. Norris, R. Mateman, A. Leinse, N. D. Bassim, A. P. Knights, and J. D. B. Bradley, "Low-loss TeO_2-coated Si_3N_4 waveguides for application in photonic integrated circuits," Opt. Express **27**, 12529–12540 (2019).
44. A. Hartung, A. M. Heidt, and H. Bartelt, "Design of all-normal dispersion microstructured optical fibers for pulse preserving supercontinuum," Opt. Express **19**, 7742–7749 (2011).
45. G. Krauss, S. Lohss, T. Hanke, A. Sell, S. Eggert, R. Huber, and A. Leitenstorfer, "Synthesis of a single cycle of light with compact erbium-doped fibre technology," Nat. Photonics **4**, 33–36 (2010).
46. M. Samoc, A. Samoc, and B. L. Davies, "Third harmonic autocorrelation and wave mixing in a thin film of poly(p-phenylenevinylene)," Opt. Express **11**, 1787–1792 (2003).
47. K. VU, S. Farahani, and S. Madden, "980 nm pumped erbium doped tellurium oxide planar rib waveguide laser and amplifier with gain in S, C and L band," Opt. Express **23**, 747–755 (2015).
48. K. M. Kiani, H. C. Frankis, H. M. Mbonde, R. Mateman, A. Leinse, A. P. Knights, and J. D. B. Bradley, "Thulium-doped tellurium oxide waveguide amplifier with 7.6 dB net gain on a silicon nitride chip," Opt. Lett. **44**, 5788–5791 (2019).
49. H. C. Frankis, H. M. Mbonde, D. B. Bonneville, C. Zhang, R. Mateman, A. Leinse, and J. D. B. Bradley, "Erbium-doped TeO_2-coated Si_3N_4 waveguide amplifiers for 5 dB net gain," Photon. Res. **8**, 127–134 (2020).
50. L. Wang, W. Xie, D. V. Thourhout, Y. Zhang, H. Yu, and S. Wang, "Nonlinear silicon nitride waveguides based on a PECVD deposition platform," Opt. Express **26**, 9646–9654 (2108).
51. S. S. Saseendran, T. D. Kongnyuy, B. Figey, F. Buja, B. Troia, S. Kerman, A. Marinins, R. Jansen, X. Rottenberg, D. S. Tezcan, and P. Soussan, "A 300 mm CMOS-compatible PECVD silicon nitride platform for integrated photonics with low loss and low process induced phase variation," in *Optical Fiber Communications Conference and Exhibition (OFC)* (2019), paper M1C.4.

52. S. J. Madden and K. T. Vu, "High performance integrated optics with tellurite glasses: status and prospects," Int. J. Appl. Glass. Sci. **3**, 289–298 (2012).
53. G. P. Agrawal, *Nonlinear Fiber Optics*, 5th ed. (Elsevier, 2012).
54. G. H. C. New and J. F. Ward, "Optical third-harmonic generation in gases," Phys. Rev. Lett. **19**, 556–572 (1967).
55. F. Kajzar and J. Messier, "Third-harmonic generation in liquids," Phys. Rev. A **32**, 2352–2363 (1985).
56. J. M. Gabriagues, "Third harmonic and three-wave sum-frequency light generation in an elliptical-core optical fiber," Opt. Lett. **8**, 183–185 (1983).
57. T. Carmon and K. Vahala, "Visible continuous emission from a silica microphotonic device by third-harmonic generation," Nat. Phys. **3**, 430–435 (2007).
58. B. Corcoran, C. Monat, C. Grillet, D. Moss, B. Eggleton, T. White, L. O'Faolain, and T. Krauss, "Green light emission in silicon through slow-light enhanced third-harmonic generation in photonic-crystal waveguides," Nat. Photonics **3**, 206–210 (2009).
59. J. S. Levy, M. A. Foster, A. L. Gaeta, and M. Lipson, "Harmonic generation in silicon nitride ring resonators," Opt. Express **19**, 11415–11421 (2011).
60. J. C. Delagnes and L. Canioni, "Third harmonic generation in periodically poled crystal," Proc. SPIE **7917**, 79171C (2011).
61. S.-Y. Hong, J. I. Dadap, N. Petrone, P.-C. Yeh, J. Hone, and R. M. Osgood, "Optical third-harmonic generation in graphene," Phys. Rev. X **3**, 021014 (2013).
62. J. B. Surya, X. Guo, C. L. Zou, and H. X. Tang, "Efficient third-harmonic generation in composite aluminum nitride/silicon nitride microrings," Optica **5**, 103–108 (2018).
63. S. Sederberg, C. J. Firby, and Elezzabi, "Efficient, broadband third-harmonic generation in silicon nanophotonic waveguides spectrally shaped by nonlinear propagation," Opt. Express **27**, 4990–5004 (2019).
64. R. Boyd, *Nonlinear Optics* (Academic, 1992), Chap. 2.
65. J. Thogersen and J. Mark, "Third harmonic generation in standard and erbium-doped fibers," Opt. Commun. **110**, 435–444 (1994).
66. N. Singh, M. Xin, N. Li, D. Vermeulen, A. Ruocco, E. S. Magden, K. Shtyrkova, E. Ippen, F. X. Kaertner, and M. R. Watts, "Silicon photonics optical frequency synthesizer," Laser Photon. Rev. **14**, 1900449 (2019).
67. H. M. Mbonde, H. C. Frankis, and J. D. B. Bradley, "Enhanced nonlinearity and engineered anomalous dispersion in TeO_2-coated Si_3N_4 waveguides," IEEE. Photon. J. **12**, 2200210 (2020).
68. N. Singh, D. Vermulen, A. Ruocco, N. Li, E. Ippen, F. X. Kartner, and M. R. Watts, "Supercontinuum generation in varying dispersion and birefringent silicon waveguide," Opt. Express **27**, 31698–31712 (2019).